Surface roughness assisted growth of vertically oriented ferroelectric SbSI nanorods

Justin Varghese,[§,†,ǁ] Colm O'Regan,[§,†,ǁ] Nitin Deepak,[†] Roger W. Whatmore,[†] and Justin D. Holmes[§,†,ǁ,*]

[§]Materials Chemistry and Analysis Group, Department of Chemistry, University College Cork, Cork, Ireland.

[†]Tyndall National Institute, University College Cork, Lee Maltings, Dyke Parade, Cork, Ireland.

[ǁ]Centre for Research on Adaptive Nanostructures and Nanodevices (CRANN), Trinity College Dublin, Dublin 2, Ireland.

KEYWORDS Nano, SbSI, Roughness, Piezoelectric, Ferroelectric, PFM.

Supporting Information Placeholder

ABSTRACT: We report the catalyst-free synthesis of arrays of *c*-axis oriented antimony sulfoiodide nanorods on anodic aluminum oxide (AAO) substrates by vapor phase deposition. The surface roughness of the AAO substrates played a decisive role in the orientation control of the SbSI nanorods produced. The as-grown SbSI nanorods were single crystalline and <001> oriented, as revealed from the x-ray diffraction and transmission electron microscopy analysis. Switching spectroscopy-piezoresponse force microscopy experiments demonstrated, for the first time, the presence of switchable ferroelectricity and piezoelectricity in individual SbSI nanorods. Ferroelectric switching in the SbSI nanorods was found to occur via a 180° domain reversal, due to the preferred orientation of the nanorods along their polar *c*-axis.

INTRODUCTION

Most of the research in nanoscale ferroelectrics and piezoelectrics has been focused primarily on oxide based perovskite materials,[1,2] with less attention given to non-oxide based systems. Many interesting ferroelectric and piezoelectric characteristics of non-oxide based systems have been reported in the literature in general,[3] among these antimony sulfoiodide (SbSI) draws attention due to its unusually high dielectric, piezoelectric and photo conducting properties.[4] SbSI is a semiconductor ferroelectric material which belongs to the V-VI-VII class of compounds and was widely studied during the 1960s and 1970s.[5-10] SbSI shows highly anisotropic behavior in many of its functional properties[11], due to polar chains of $(SbSI)_\infty$ which run parallel to the *c*-axis.[12] This anisotropy accounts for its superior functional characteristics, such as a high peak pyroelectric coefficient (6×10^{-2} C m^{-2} K^{-1}),[13] dielectric constant (~50,000),[4] refractive index (~4.5),[14] and piezoelectric coefficient (2000 pC N^{-1}),[10] along the polar axis in single crystalline form.[12] These versatile functional properties of SbSI could lead to its use in many applications such as thermal imaging,[15] non-linear optics,[16] and mechanical actuation.[17]

However, although promising for many potential uses, the difficulty in obtaining vertically aligned phase pure SbSI single crystals has put severe constraints on its real applicability.[15] The International Technology Roadmap for Semiconductors (ITRS) has identified the need for new nanostructured ferroelectric materials with significantly-improved properties to meet future technology requirements.[18] As all of the interesting functional properties of SbSI are maximized along its *c*-axis, the synthesis of vertically (*c*-axis) oriented SbSI nanostructures should allow exploitation of these superior properties. Previously, SbSI nanorods and nanowires have been synthesized by hydrothermal[19,20] and sonochemical[21] routes. Vapor deposition[22,23] and pulsed laser deposition[15,24] methods have been widely used for making SbSI crystals and thin films. Whilst some of these methods[8,15] have been successful in producing *c*-axis oriented thin films, there been no literature reports to date on the synthesis of vertically-aligned SbSI nanostructures. Most of the approaches reported for preparing one-dimensional SbSI materials result in randomly-oriented, large-grained or discontinuous structures, due to the large energy barrier for nucleation of SbSI on many substrates. The surface roughness of a substrate plays a crucial role in controlling the energy barrier for nucleation and orientation of the nanostructures, especially nanowires and nanorods. Recently, vertically aligned arrays of ZnO nanorods were synthesized on chemically etched sapphire substrates by a catalyst-free vapor-solid (VS) growth approach.[25,26] The vertical alignment of ZnO was caused by the assistance of irregularities, or roughness, present on the surface of the sapphire substrates. The surface roughness on a substrate can act as nucleation centers which reduce the nucleation barrier, improving oriented growth.[25,26] Based on this hypothesis, we have utilized the inherent surface roughness of anodic aluminum oxide/titanium/silicon (AAO/Ti/Si) substrates to assist the growth of vertically aligned SbSI nanorods by vapor phase deposition. In addition, the nanoscale piezoelectric and ferroe-

lectric characteristics of the SbSI nanorods were studied using piezoresponse force microscopy (PFM), allowing the ferroelectric and piezoelectric functionality of individual nanostructures to be characterized on a one-to-one basis.

EXPERIMENTAL METHODS

AAO/Ti/Si substrates were prepared by the two-step anodization[27] of Al/Ti/Si substrates at 40 V in 0.3 M oxalic acid, at 4 °C. SbSI nanorods were synthesized on AAO/Ti/Si substrates by vapor phase deposition of a mixture of Sb_2S_3 and SbI_3 powders (1:0.8 molar ratios). The deposition was carried out in a two-zone tube furnace with the source placed in the middle of a quartz tube, while the substrate was placed downstream at an optimum distance of ~15 cm from the source. The quartz tube was then evacuated (~10^{-4} Torr) for 1 h to attain a steady vacuum and then sealed. The source and substrate zone temperature were then raised to 400 and 250 °C respectively, at a heating ramp rate of 1 °C min^{-1} and the deposition was carried out for 1 h. A control experiment was conducted with a Si (001) substrate under similar conditions.

The phase composition and purity of the SbSI nanostructures synthesized was investigated by x-ray diffraction (XRD), on a Philips X'Pert diffractometer using Cu Kα1 radiation with an anode current of 35 mA and an accelerating voltage of 40 kV. The morphology of the SbSI samples produced was analyzed using a FEI Quanta 650 FEG-SEM. High-resolution transmission electron microscopy (HRTEM) analysis of the samples was performed on a JEOL-JEM 2100 TEM operated at 200 kV, fitted with an Oxford INCA EDX detector. Selected area electron diffraction (SAED) was obtained using HRTEM along the [010] zone-axis of the SbSI nanorods. The SbSI nanorods were dispersed on a conducting platinum substrate for PFM measurements. The nanoscale ferroelectric and piezoelectric properties of the SbSI nanorods were then analyzed by dual resonance tracking (DART) switching spectroscopy- piezoresponse force microscopy (SS-PFM, MFP-3D™ software, Asylum Research, Santa Barbara, CA) using a calibrated conductive cantilever (AC240TM platinum coated silicon tip, Olympus).

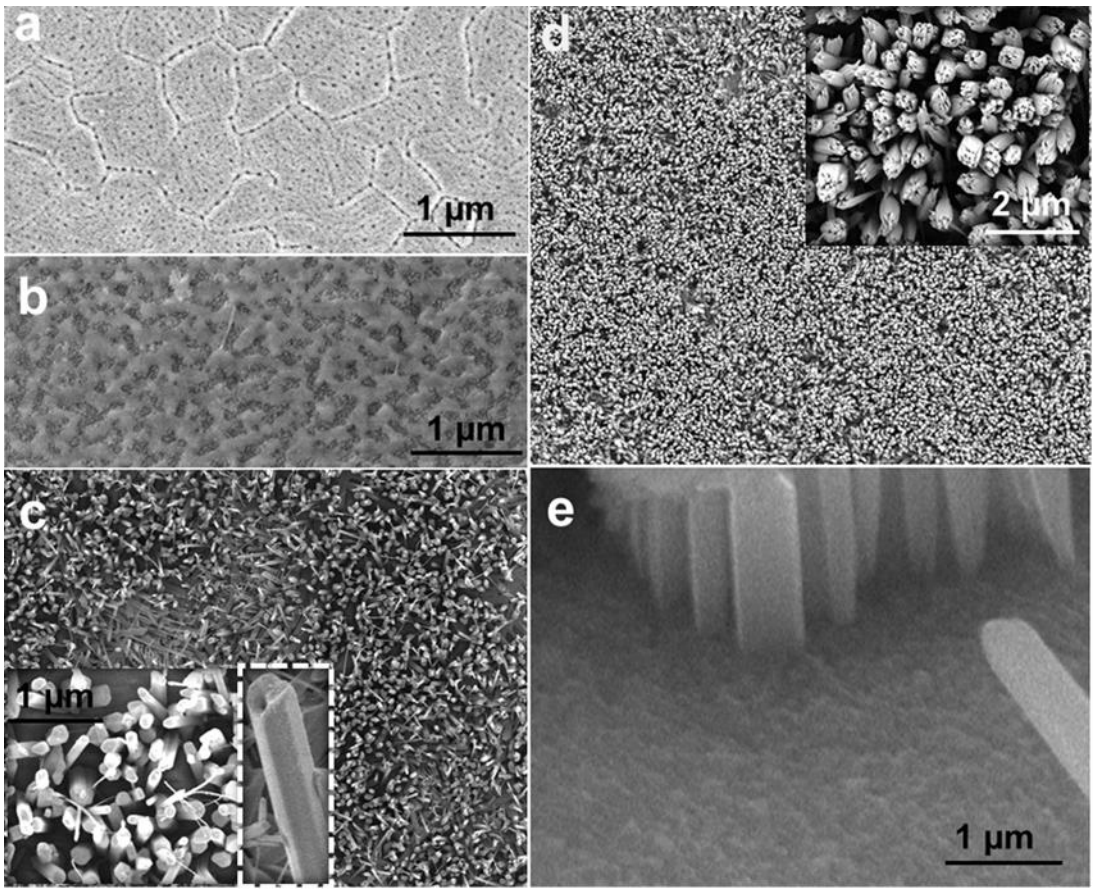

Figure 1. SEM images showing (a) plan-view image of an AAO/Ti/Si substrate, (b) islands of $(SbI_3)_x(Sb_2S_3)_{1-x}$ formed at170 °C on an AAO/Ti/Si substrate, (c) vertical SbSI nanorods formed at 250 °C (Insets show magnified plan-view and side-view SEM image of SbSI nanorods), (d) vertical SbSI nanorod clusters formed at 275 °C, and (e) side-view of SbSI nanorods formed on an AAO/Ti/Si substrate at 250 °C.

RESULTS AND DISCUSSION

The change in the morphology of the synthesized SbSI nanostructures as a function of temperature is shown in Figure 1. The surface morphology of a bare AAO surface on a Ti/Si substrate (Figure 1(a)) shows pores with diameters ranging between 20 to 50 nm, including grain boundaries. These pores and grain boundaries give the AAO its rough surface. SbSI forms by a gaseous phase reaction between Sb_2S_3 and SbI_3 at a source temperature of 400 °C to form $(SbI_3)_x(Sb_2S_3)_{1-x}$,[23,28] which is then transported across a temperature gradient onto an AAO/Ti/Si substrate. The onset of nucleation of SbSI starts close to 160 °C, under conditions close to the critical saturation for the condensation of $(SbI_3)_x(Sb_2S_3)_{1-x}$.[23,28] As shown in Figure 1(b), SbSI starts nucleating at a substrate temperature of 170 °C in the form of tiny islands of $(SbI_3)_x(Sb_2S_3)_{1-x}$ condensate,[23,28] with a mean lateral size of ~ 200 to 300 nm. As the substrate temperature is increased to 250 °C, vertically oriented SbSI nanorods with a mean length of ~ 3 µm and diameter range between 150 to 300 nm were formed on the surface of the AAO/Ti/Si substrate (Figure 1(c)). Upon increasing the substrate temperature to 275 °C, the SbSI nanorods tend to coalesce to form vertically oriented SbSI nanorod clusters with a mean length of ~ 3 µm and diameter of 600 nm (Figure 1(d)). The coverage and density of the vertical SbSI crystallites on the AAO/Ti/Si substrates increases as the substrate temperature is increased from 250 to 275 °C since a higher temperature could increase the migration rate of SbSI species, promoting a high uniform distribution of SbSI on the surface.[29] Figure 1(e) shows the side-view of SbSI nanorods, clearly indicating that nucleation starts from the AAO surface. In this work, the optimum temperature to obtain phase pure SbSI was found to be 250 °C. Deposition temperatures lower and higher than 250 °C resulted in SbI_3 rich SbSI and non-stoichiometric SbSI respectively. Since no catalytic particle was observed on the tips of the SbSI nanorods (see inset Figure 1(c)), the nanorod growth process occurred via a self-catalyzed vapor-solid growth mechanism.

The phase purity of the as-synthesized SbSI nanorods was confirmed by XRD analysis. The XRD pattern of SbSI nanorods grown from an AAO/Ti/Si substrate, at a reaction temperature of 250 °C, is shown in Figure 2(a) and can be indexed to orthorhombic SbSI (space group, $Pna2_1$; PDF no. 88-2407), displaying a high intensity (002) reflection at 2θ = 44.3°; indicative of predominant *c*-axis oriented growth. To further confirm the *c*-axis oriented growth, TEM analysis has undertaken on isolated SbSI nanorods. TEM image of a SbSI nanorod (Figure 2(c)) reveals the single crystalline nature of a nanorod with a predominant growth direction along the <001> axis, confirming that the *c*-axis is normal to the substrate plane. The measured lattice fringe spacing of 0.648 nm corresponds to the (110) plane of the nanorod. Selected area electron diffraction (SAED) was used to further confirm the *c*-axis orientation of the SbSI nanorods. The electron diffraction pattern, obtained in the [010] zone axis, (inset in Figure 2(c)) further reiterates the single crystalline nature and dominant <001> growth of the nanorods. The lattice fringe spacing and angles between planes in the SAED pattern can be indexed to orthorhombic SbSI. The composition of individual SbSI nanorods grown at 250 °C, determined by EDX analysis (Figure 2(b)), was found to be $SbSI_{0.95}$, with 33.9 % Sb, 34.0% S and 32.2% I, close to the expected stoichiometry. SbSI nanorods formed at 275 °C were found to be slightly non-stoichiometric, with a composition of $SbS_{0.9}I_{0.89}$ (see supporting information), due to the partial decomposition of SbSI.[22]

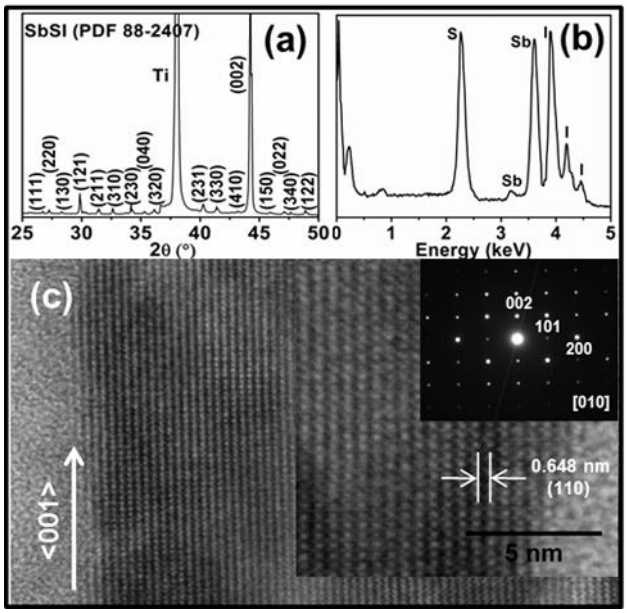

Figure 2. (a) XRD pattern of SbSI nanorods formed at 250 °C on an AAO/Ti/Si substrate, indexed to orthorhombic SbSI (PDF No: 88-2407), (b) EDX spectrum of an individual SbSI nanorod, and (c) TEM image of a SbSI nanorod showing preferential <001> oriented growth (inset showing high resolution images of lattice fringes and SAED pattern obtained along [010] zone axis); the marked lattice fringe spacing of 0.648 nm corresponds to the (110) lattice plane of SbSI.

To study the influence of surface roughness on the alignment of SbSI nanorods, a control experiment was carried out using a Si (001) substrate (Figure 3(a)), under similar deposition conditions to those used with the AAO/Ti/Si substrates. Figure 3(b) shows an SEM image of SbSI formed on a Si substrate at a deposition temperature of 250 °C. Randomly oriented one dimensional SbSI crystallites, with lengths between ~ 5 to 7 µm and width between ~ 600 to 700 nm, were observed on the Si substrate, highlighting that the substrate surface plays a crucial role in orienting the SbSI nanostructures. SbSI crystallites formed on smooth Si substrates preferred to align parallel to the substrate plane (Figures 3(b) and 3(c)), compared to the perpendicular alignment observed with the rough AAO/Ti/Si substrates (Figure 1(c) and 1(d)). However, SbSI crystals deposited on Si and AAO/Ti/Si substrates have a similar composition and one-dimensional morphology, but differ in their alignment. The one-dimensional orientation of the nanorods is attributed to the inherently fast growth of the SbSI crystals along their *c*-axis compared to their *a*-*b* planes.[12] The XRD pattern (Figure 3(d)) obtained for the deposited films on Si substrate can be indexed to orthorhombic SbSI (PDF no: 74-2245), with a distinct peak at 2θ = 32.8°, corresponding to the (310) reflection plane.

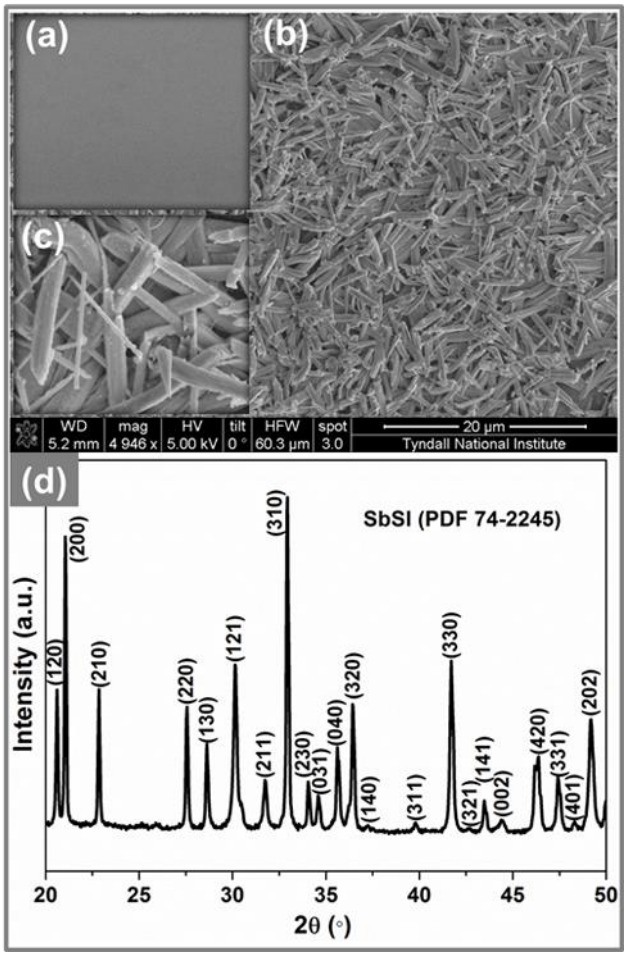

Figure 3. Plan-view SEM images of (a) a bare Si (001) substrate, (b) SbSI nanorods formed on a Si substrate at a temperature of 250 °C, (c) zoomed-in image of SbSI crystallites and (d) XRD pattern of crystallites formed on a Si substrate, indexed to orthorhombic SbSI (PDF No: 74-2245).

The difference in the alignment of SbSI crystallites formed on AAO/Ti/Si and Si substrates can be explained by taking into account the surface roughness of these substrates. The rough surface of the AAO substrates (pores and grain boundaries) provides enough nucleation centers for the vertical growth of SbSI compared to a smooth Si substrate, due to the lower critical energy required for nuclei formation on a rough substrate.[22,30] AFM surface roughness analysis showed that an as-synthesized AAO/Ti/Si substrates had a root mean square surface roughness of 9.03 ± 0.50 nm compared to 0.81 ± 0.02 nm for Si substrates. In comparison with the smooth Si substrate, an AAO/Ti/Si substrate provides more binding sites for the vertical growth of SbSI, accounting for the initial formation of islands of $(SbI_3)_x(Sb_2S_3)_{1-x}$ (Figure 1(b)), with no such deposition observed on Si substrates at the same temperature. These islands of $(SbI_3)_x(Sb_2S_3)_{1-x}$ act as nucleation centers for the vertical growth of SbSI nanorods. Once the nucleation occurs, the continued supply of incoming SbSI vapors result in one-dimensional growth.[31] As seen in Figure 1(e), SbSI nanorods were nucleated and grown directly on the upper surface of the AAO template. Similar reasoning was applied for the formation of vertically aligned ZnO nanorods on chemically etched sapphire substrate,[25,26] SiC/AlSiC core-shell nanowires on AAO[32] membranes and V_2O_5 nanowires on chemically etched Si (001) substrates[31]. Due to the amorphous nature of AAO, epitaxial growth of SbSI can be excluded.

To compare the preferential orientation of the SbSI nanorods deposited on AAO/Ti/Si and Si substrates two XRD peaks of SbSI, (330) and (002), were studied. These peaks were chosen since the normal direction to the (002) plane corresponds to the *c*-axis and is parallel to the (330) plane, which is suitable to determine the vertical alignment of SbSI.[33] Figure 4 shows a comparison of the change in intensities of the (330) and (002) XRD peaks obtained for SbSI deposited, at 250 °C, on Si and AAO/Ti/Si substrates. The (330) and (002) diffraction peaks of SbSI appear at 41.6° and 44.3° (2θ) respectively. The peak intensity from the (002) diffraction plane of the SbSI crystals formed on a Si substrate (Figure 4(a)) was very weak compared to that from the nanorods formed on an AAO/Ti/Si substrate (Figure 4(b)). The high intensity (330) diffraction peak and low intensity (002) peak highlights that the *c*-axis of the SbSI crystallites grown on Si were aligned parallel to the substrate plane. In contrast, XRD analysis of SbSI nanorods deposited on AAO/Ti/Si substrates showed intense (002) and weak (310) reflections respectively, due to preferential vertical alignment of the SbSI nanorods along their *c*-axis.

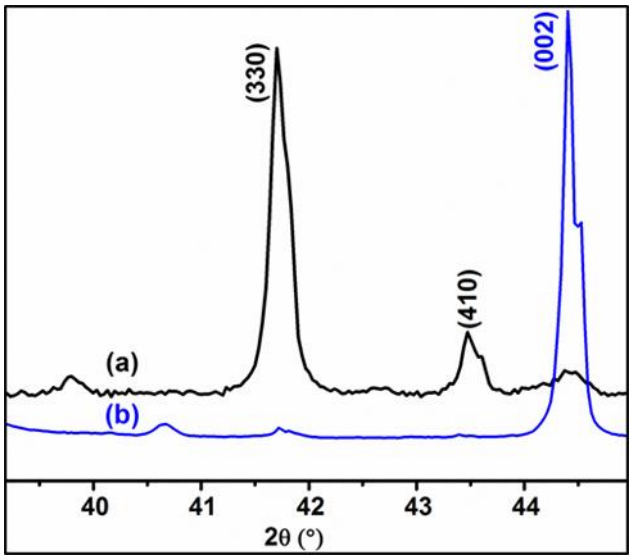

Figure 4. XRD patterns showing the influence of substrate on the degree of *c*-axis orientation of SbSI crystallites. (a) SbSI crystallites deposited on a Si substrate at 250 °C, and (b) SbSI nanorods formed on AAO/Ti/Si substrate at 250 °C.

One of the most influential factors determining the morphology of the SbSI crystals deposited on a given substrate, is the relative surface energies of various growth facets at the deposition conditions employed.[34] The inset in Figure 1(c) indicates that the SbSI nanorods are faceted, which can be attributed to the polar nature of the SbSI crystals. Polar surfaces are generally stabilized by surface reconstruction or faceting.[34] During SbSI formation, after an initial period of nucleation, SbSI tends to form 1D structures because the nanorod

formation can maximize the areas of the {110}, {010} and {100} facets, which have a lower free energy compared to {002} facets.[35,36] Along the [001] direction, the growth of SbSI can take place without the formation of a 2D nuclei since its orthorhombic structure ($Pna2_1$) possess a 2_1 screw axis in this direction.[37]

The nanoscale piezoelectric and ferroelectric properties of SbSI nanorods grown at 250 °C on AAO/Ti/Si substrates were studied, for the first time, using piezoresponse force microscopy (PFM) in contact mode. Compared to bulk techniques, PFM has the advantage of being able to visualize the ferroelectric domain dynamics, polarization switching and quantification of piezoelectric responses of individual nanostructures.[38-41] The PFM ferroelectric and piezoelectric response obtained from a cluster of SbSI nanorods, 2.0 × 2.0 μm^2, dispersed on a conducting platinum substrate is shown in Figure 5. The PFM topography, piezoresponse amplitude and ferroelectric domain phase images obtained for SbSI nanorods are shown in Figures 5(a) to (c) respectively. The piezo response can be clearly seen from the bright and dark amplitude contrast of the nanorods shown in Figure 5(b). The presence of the bright white contrast is evidence of a piezoresponse in the SbSI nanorods, due to an out-of-plane displacement along the polar *c*-axis. The PFM phase image (Figure 5(c)) of the SbSI nanorods clearly shows the presence of ferroelectric domains present in the material. Different orientations of the polar axis of adjacent domains in SbSI nanorods lead to multi-domain contrast. This multi-domain structure is formed as a result of the differing level of polarity present in individual ferroelectric domains.[38]

The primary feature of a ferroelectric material is the reversal of spontaneous polarization under the application of an applied electric field. Piezoresponse force microscopy (PFM) has become a standard technique to analyze the local ferroelectric/piezoelectric switching properties of nanoscale materials.[38-40] An advanced version of PFM called switching spectroscopy PFM (SS-PFM) allows the acquisition of ferroelectric and piezoelectric switching hysteresis loops from a point on a nanostructure. In our study, hysteresis loops were obtained by positioning the PFM conducting tip on top of a SbSI nanorod and applying an AC voltage of 3.3 V plus a DC bias of ±44 V simultaneously across the nanorod and the back electrode. Figures 6(a) and (b) show the phase and piezoresponse switching hysteresis obtained from a single SbSI nanorod, by positioning the tip in the center of the top edge of a nanorod (Figure 6(a), red dot in the inset image). Positioning the tip on the (002) plane of the SbSI nanorod allows the measurement of the piezoresponse along the polar *c*-axis. The square shape phase-voltage hysteresis (Figure 6(a)) curve obtained gives strong evidence for the presence of switchable ferroelectricity in SbSI nanorods. The 180° phase difference observed during switching (Figure 6(a)) can be attributed to the presence of 180° ferroelectric polarization present along the *c*-axis in the SbSI nanorod. Due to the <001> orientation of the SbSI nanorods, the polarization change occurs mostly along the *c*-axis of the nanorod and thus results in the formation of two oppositely oriented (180°) ferroelectric domains along the polar axis. Similar results have previously been reported by us for <001> oriented Sb_2S_3 nanowires.[42] Figure 6(b) depicts the normalized piezoresponse hysteresis response obtained for a SbSI nanorod, from the same location as that of the phase hysteresis. The inset image in Figure 6(b) shows the classical ferroelectric loop acquired from the SbSI nanorod, which is a signature of the presence of switchable piezoelectric response in the material.[39]

The effective piezoelectric coefficient d_{33}(eff) for the SbSI nanorods, calculated using equation[38,40], $d_{33} = A/V_{ac}Q_f$, where A is the maximum amplitude, V_{ac} is the applied AC voltage and Q_f is the quality factor (obtained during the PFM measurement and depends solely on the tip-sample surface interaction), was found to ~ 12 pm V^{-1}.[10] The difficulty related to positioning the PFM tip at a specific location on top of a SbSI nanorod surface, due to tip shift, put constraints on quantifying the piezoelectric response and limits our study to a qualitative view point. Figure 6(c) illustrates the changes observed in domains during ferroelectric switching of a single SbSI nanorod when a DC bias of ±44 V was applied. The applied bias induces a reversal of the ferroelectric domain structure and provides clear evidence for the presence of switchable ferroelectricity in the SbSI nanorods.

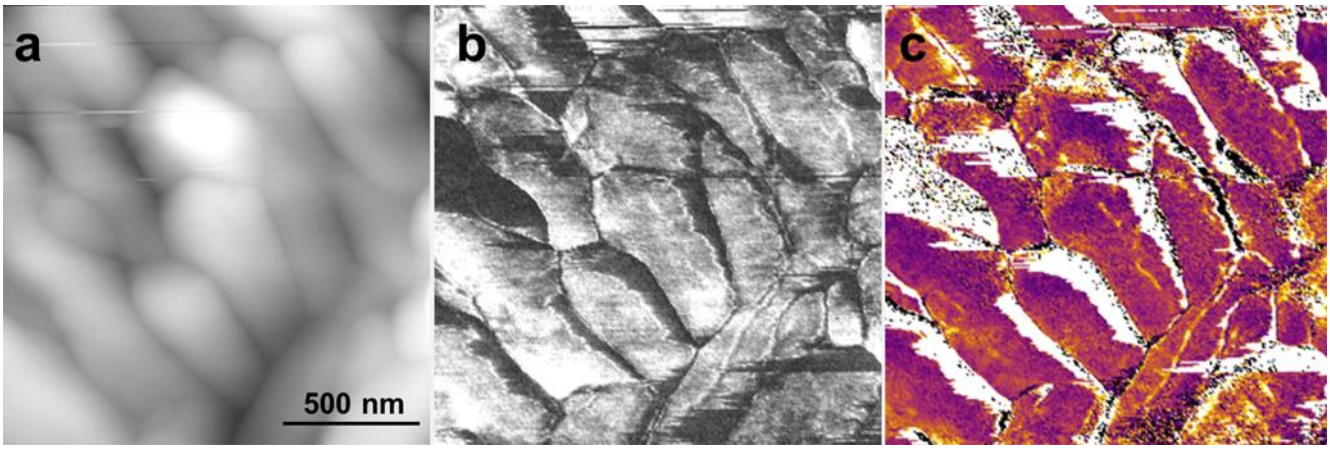

Figure 5. PFM images of SbSI nanorods dispersed on a conducting platinum substrate, showing (a) height, (b) amplitude, and (c) phase profiles SbSI nanorods grown at 250 °C on AAO/Ti/Si substrate.

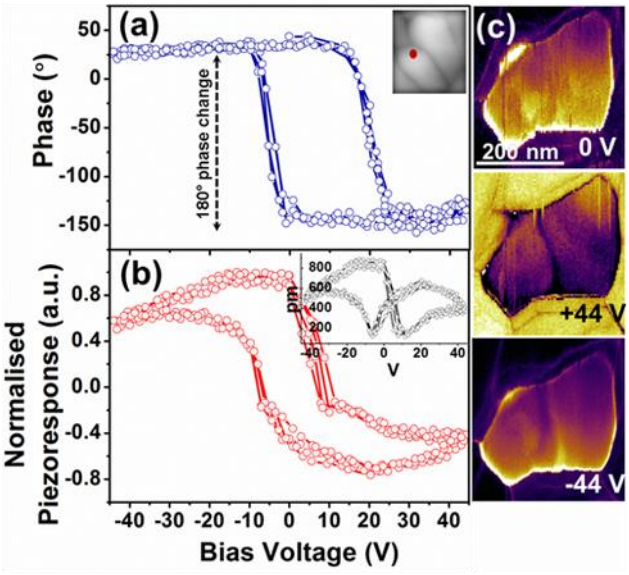

Figure 6. (a) SS-PFM phase-switching hysteresis, (the red dot in the inset image shows the location of the tip on the SbSI nanorod during the hysteresis loop acquisition), (b) normalized piezo-switching hysteresis (inset shows the actual butterfly shaped piezoresponse hysteresis loop), loops acquired from an individual SbSI nanorod and (c) SS-PFM phase images showing ferroelectric domain switching of a selected SbSI nanorod before and after domain switching, by applying a bias voltage of ±44V.

The presence of ferroelectricity in SbSI can be attributed to its orthorhombic structure with the polar space group $Pna2_1$, at room temperature. SbSI has a phase transition or Curie temperature (T_C) of ~ 22 °C at which it undergoes a phase transition from the ferroelectric $Pna2_1$ phase to the paraelectric Pnma phase.[4,11] The ferroelectric and piezoelectric switching, under the application of an applied bias, in SbSI is associated with the alternating arrangement of polar double chains $[(SbSI)_\infty]_2$ parallel to the [001] axis.[11] The asymmetric arrangement of these double chains creates disorder of the Sb atoms and polarity in the SbSI crystal, which in turn results in unidirectional polarization along the polar *c*-axis due to <001> orientation of the SbSI nanorods, accounting for their ferroelectric and piezoelectric behavior.

CONCLUSION

In summary, arrays of *c*-axis oriented SbSI nanorods were synthesized by a surface roughness assisted vapor deposition method on AAO/Ti/Si substrates. The growth of SbSI nanorods proceeded via a seedless vapor-solid mechanism. XRD and TEM-SAED analysis of the as-synthesized SbSI nanorods confirmed their single crystalline nature and <001> oriented preferred growth. Surface roughness of the AAO substrate played a crucial role in vertically orienting the SbSI nanorods, by providing a large number of binding centers for nucleation. PFM studies revealed the presence of switchable ferroelectric and piezoelectric responses in individual SbSI nanorods. A 180° phase difference was observed during ferroelectric switching which could be attributed to the presence of the formation of two oppositely oriented (180°) ferroelectric domains, due to the *c*-axis oriented single crystalline nature of the SbSI nanorods.

ASSOCIATED CONTENT

XRD pattern and EDX spectrum obtained for SbSI nanorods formed on an AAO/Ti/Si substrate at a growth temperature of 275 °C. This material is available free of charge via the Internet at http://pubs.acs.org.

AUTHOR INFORMATION

Corresponding Author

* Justin D. Holmes, E-mail: j.holmes@ucc.ie, Tel: +353 (0)21 4903608; Fax: +353 (0)21 4274097.

ACKNOWLEDGMENT

This work was supported by Science Foundation Ireland (SFI) under the FORME Strategic Research Cluster Award (Project 07/SRC/I1172). This research was also enabled by the Higher Education Authority Program for Research in Third Level Institutions (2007-2011) via the INSPIRE program. The authors acknowledge the facilities of, and technical assistance from the staff at, Electron Microscopy and Analysis Facility (EMAF) at Tyndall National Institute.

ABBREVIATIONS

SbSI, antimony sulfoiodide; AAO, anodic aluminum oxide; PFM, piezoresponse force microscopy.

REFERENCES

(1) Rørvik, P. M.; Grande, T.; Einarsrud, M.-A. *Adv. Mater.* **2011**, *23*, 4007-4034.
(2) Handoko, A. D.; Goh, G. K. L. *Science of Advanced Materials* **2010**, *2*, 16-34.
(3) Mitsui, T. In *Springer Handbook of Condensed Matter and Materials Data*; Martienssen, W., Warlimont, H., Eds.; Springer: Berlin Heidelberg, 2005; pp 903-936.
(4) Fatuzzo, E.; Nitsche, R.; Harbeke, G.; Ruppel, W.; Roetschi, H.; Merz, W. J. *Physical Review* **1962**, *127*, 2036-2037.
(5) Kern, R. *J. Phys. Chem. Solids* **1962**, *23*, 249-253.
(6) Hamano, K.; Nakamura, T.; Ishibash.Y; Ooyane, T. *J. Phys. Soc. Jpn.* **1965**, *20*, 1886-1888.
(7) Imai, K.; Kawada, S.; Ida, M. *J. Phys. Soc. Jpn.* **1966**, *21*, 1855-1860.
(8) Yoshida, M.; Yamanaka, K.; Hamakawa, Y. *Jpn J Appl Phys* **1973**, *12*, 1699-1705.
(9) Sime, R. J. *J. Phys. Chem.* **1963**, *67*, 501-503.
(10) Berlincourt, D.; Nitsche, R.; Merz, W. J.; Jaffe, H. *Appl. Phys. Lett.* **1964**, *4*, 61-63.
(11) Audzijonis, A.; Grigas, J.; Kajokas, A.; Kvedaravicius, S.; Paulikas, V. *Ferroelectrics* **1998**, *219*, 37-45.
(12) In *Landolt-Börnstein - Group III Condensed Matter*; Madelung, O., Rössler, U., Schulz, M., Eds.; Springer-Verlag, 1998; Vol. III/17E-17F-41C.
(13) Bhalla, A. S.; Newnham, R. E.; Cross, L. E.; Dougherty, J. P.; Smith, W. A. *Ferroelectrics* **1981**, *33*, 3-7.
(14) Johannes, R.; Haas, W. *Appl. Opt.* **1967**, *6*, 1059-1061.
(15) Kotru, S.; Liu, W.; Pandey, R. K. In *Proceedings of the 12th IEEE International Symposium on Applications of Ferroelectrics, ISAF 2000.*, 2000; Vol. 1; pp 231-234.
(16) Brown, M. P.; Newnham, S. J.; Smith, P. W. In *Seventh International Conference on Dielectric Materials, Measurements and Applications (Conf. Publ. No. 430)*, 1996; pp 76-81.

(17) Nowak, M.; Mroczek, P.; Duka, P.; Kidawa, A.; Szperlich, P.; Grabowski, A.; Szala, J.; Moskal, G. *Sensors and Actuators A: Physical* **2009**, *150*, 251-256.
(18) *The International Technology Roadmap for Semiconductors: 2011 Edition, Emerging research materials and Emerging research devices;* http://www.itrs.net/Links/2011ITRS/2011Chapters/2011ERM.pdf, http://www.itrs.net/Links/2011ITRS/2011Chapters/2011ERD.pdf.
(19) Wang, C.; Tang, K.; Yang, Q.; Hai, B.; Shen, G.; An, C.; Yu, W.; Qian, Y. *Inorg. Chem. Commun.* **2001**, *4*, 339-341.
(20) Yang, Q.; Tang, K.; Wang, C.; Hai, B.; Shen, G.; An, C.; Zhang, C.; Qian, Y. *J. Cryst. Growth* **2001**, *233*, 774-778.
(21) Nowak, M.; Szperlich, P.; Bober, Ł.; Szala, J.; Moskal, G.; Stróż, D. *Ultrason. Sonochem.* **2008**, *15*, 709-716.
(22) Solayappan, N.; Raina, K. K.; Pandey, R. K.; Varshney, U. *J. Mater. Res.* **1997**, *12*, 825-832.
(23) Dziuba, Z. *J. Cryst. Growth* **1976**, *35*, 340-342.
(24) Surthi, S.; Kotru, S.; Pandey, R. K. *J. Mater. Sci. Lett.* **2003**, *22*, 591-593.
(25) Ho, S.-T.; Chen, K.-C.; Chen, H.-A.; Lin, H.-Y.; Cheng, C.-Y.; Lin, H.-N. *Chem. Mater.* **2007**, *19*, 4083-4086.
(26) Ho, S.-T.; Wang, C.-Y.; Liu, H.-L.; Lin, H.-N. *Chem. Phys. Lett.* **2008**, *463*, 141-144.
(27) Masuda, H.; Fukuda, K. *Science* **1995**, *268*, 1466-1468.
(28) Balarew, C.; Ivanova, M. *Cryst. Res. Technol.* **1986**, *21*, K171-K175.
(29) Liu, C.; Hu, Z.; Wu, Q.; Wang, X.; Chen, Y.; Sang, H.; Zhu, J.; Deng, S.; Xu, N. *J. Am. Chem. Soc.* **2005**, *127*, 1318-1322.
(30) Cao, G. *Nanostructures and Nanomaterials : Synthesis, Properties, and Applications*; 1 ed.; Imperial College Press: London, 2004; Vol. 1.
(31) Tien, L.-C.; Chen, Y.-J. *Appl. Surf. Sci.* **2012**, *258*, 3584-3588.
(32) Fang, J.; Aharonovich, I.; Levchenko, I.; Ostrikov, K.; Spizzirri, P. G.; Rubanov, S.; Prawer, S. *Cryst Growth Des* **2012**, *12*, 2917-2922.
(33) Miyabe, S.; Nakano, T.; Ishimoto, T.; Takano, N.; Adachi, T.; Iwaki, H.; Kobayashi, A.; Takaoka, K.; Urnakoshi, Y. *Materials Transactions* **2007**, *48*, 343-347.
(34) Iwanaga, H.; Fujii, M.; Takeuchi, S. *Phase Transitions* **1998**, *66*, 147-165.
(35) Zadorozhnaya, L. A.; Lyachovitskaya, V. A.; Givargizov, E. I.; Belyaev, L. M. *J. Cryst. Growth* **1977**, *41*, 61-66.
(36) Wang, L.; Zhang, X.; Zhao, S.; Zhou, G.; Zhou, Y.; Qi, J. *Appl. Phys. Lett.* **2005**, *86*, 024108-3.
(37) Arivuoli, D.; Gnanam, F. D.; Ramasamy, P. *J. Cryst. Growth* **1986**, *79*, 432-435.
(38) Balke, N.; Bdikin, I.; Kalinin, S. V.; Kholkin, A. L. *J. Am. Ceram. Soc.* **2009**, *92*, 1629-1647.
(39) Jesse, S.; Baddorf, A. P.; Kalinin, S. V. *Appl. Phys. Lett.* **2006**, *88*, 062908.
(40) Jesse, S.; Lee, H. N.; Kalinin, S. V. *Rev. Sci. Instrum.* **2006**, *77*, 073702.
(41) Rodriguez, B. J.; Jesse, S.; Alexe, M.; Kalinin, S. V. *Adv. Mater.* **2008**, *20*, 109-114.
(42) Varghese, J.; Barth, S.; Keeney, L.; Whatmore, R. W.; Holmes, J. D. *Nano Lett.* **2012**, *12*, 868-872.

Table of Content artwork